Optimized Precoders for Massive MIMO OFDM Dual Radar-Communication Systems

Murat Temiz, *Member, IEEE*, Emad Alsusa, *Senior Member, IEEE,* and Mohammed W. Baidas, *Senior Member, IEEE*

***Abstract*—This paper considers the optimization of a dual-functional radar and communication (RadCom) system with the objective is to maximize its sum-rate (SR) and energy-efficiency (EE) while satisfying certain radar target detection and data rate per user requirements. To this end, novel RadCom precoder schemes that can exploit downlink radar interference are devised for massive multiple-input-multiple-output (MIMO) orthogonal frequency-division multiplexing (OFDM) systems. First, the communication capacity and radar detection performance metrics of these schemes are analytically evaluated. Then, using the derived results, optimum beam power allocation schemes are deduced to maximize SR and EE with modest computational complexity. The validity of the analytical results is confirmed via matching computer simulations. It is also shown that, compared to benchmark techniques, the devised precoders can achieve substantial improvements in terms of both SR and EE.**

***Index Terms*—Energy-Efficiency, massive MIMO, radar and communication, OFDM radar, power allocation**

I. Introduction

Today's radar and communication systems require wideband frequency resources to provide high-accuracy target detection and high date-rate communications. The co-existence of these systems in what has become a congested spectrum is precarious due to the inevitable interference between them. Several studies have explored how to facilitate such coexistence, particularly through designing robust waveforms that are less prone to interference [1], [2]. In one of the early works, opportunistic spectrum sharing was proposed, in which the communication and radar systems transmit at the same time and frequency if the interference is within tolerable levels [3]. Spectrum sharing has gained more interest with recent MIMO advancements where spatial diversity is utilized. In such systems, the radar waveform is beamformed in the null spaces of the communication interference channel to reduce its impact on the network [4]. This method was further improved by selecting the optimum base-station (BS) cluster with the most null-spaces [5]. The authors in [6] proposed incorporating the design of MIMO matrix completion radars with the communication covariance matrix to reduce their mutual interference. On the other hand, [7] proposed reducing the communication systems interference on radars by exploiting constructive interference within the communication system to minimize their transmit power. Conversely, in [8], joint radar waveform and communication covariance matrix design was also investigated to maximize the communication data-rate by minimizing the radar energy towards the communication receiver. An OFDM based radar waveform was also considered in [9] where the subcarriers are distributed between the radar and communication system.

While the above mentioned studies concern relatively co-located radar and communication systems (e.g. a long-range radar and a communication cell), various current applications require simultaneous communications and radar sensing to safely and continuously perform their tasks. These include commercial flight control systems, automotive radar and communication systems, as well as intelligent transportation systems which require the vehicles to sense the environment and communicate with their surroundings to enable autonomous and safe driving conditions as well as infotainment, [1]. To achieve their dual functionality, radar and communication systems require wideband frequency resources and an abundance of energy [18], [24]. As such, there has been increasing interest in developing solutions to enhance these platforms. One such solution considered designing an integrated waveform that can be realized using linear frequency modulation (LFM), continuous phase modulation (CPM) [10], quadrature amplitude modulation (QAM) [11], or OFDM waveforms, [12], [13]. However, using such waveforms imposes a performance trade-off between the radar and the communication system, as well as restricting beamforming or/and multi-user communication. Furthermore, intrapulse radar-embedded communications were also considered to provide dual-function systems, and optimized via multiobjective optimization to maximize the signal-to-interference ratio and minimize the correlation index [14], [15]. In contrast, other approaches considered utilizing spatial diversity in massive MIMO. For example, in [16], two beamforming techniques for downlink RadCom are proposed, one is based on dividing the BS antennas into two separate groups for the communication and radar, with the radar waveform designed to fall into the null-space of the communication channels; in the second method all the antennas are used to beamform the waveform towards the user equipments (UEs) and targets by treating the targets as virtual UEs. Optimum waveform design for the second method was proposed in [17].

The application of OFDM waveforms in vehicular system RadComs has recently gained popularity due to offering desirable signal processing flexibility [18], [25]. The design of such waveforms for vehicular radars were comprehensively studied in [18] and [19]. Other techniques that follow this approach are proposed in [20] where an interference cancellation algorithm is recommended for mitigating the mutual interference caused by the Doppler shift or/and non-ideal hardware components.

M. Temiz and E. Alsusa are with the School of Electrical and Electronic Engineering, University of Manchester, Manchester, UK (e-mail:{murat.temiz, e.alsusa}@manchester.ac.uk).
M. W. Baidas is with the Department of Electrical Engineering, Kuwait University, Kuwait (e-mail: m.baidas@ku.edu.kw)

Table I
COMPARISON OF CO-LOCATED OR DUAL-FUNCTION RADAR-COMMUNICATION STUDIES

Study	Method	Notes
[3]	Opportunistic spectrum sharing	Tolerable level of interference
[4], [5]	Null space beamforming of the radar waveform	Proposed for MIMO systems
[7]	Exploiting the constructive interference	Proposed for MIMO systems
[10]–[13]	Integrated waveform for both functions	Utilizing LFM, CPM, and OFDM waveforms
[14], [15]	Intrapulse radar-embedded communications	Utilizing pulsed radar waveforms
[16], [17]	Dual-function RadCom design	Proposed for MIMO systems
[18]–[20]	OFDM waveform based RadCom system	Utilizing separate subcarriers
[21]	OFDM waveform based massive MIMO RadCom systems	Utilizing the same subcarriers
[22], [23]	Optimization of RadCom systems	Subcarrier selection and power allocation
This study	Optimization of massive MIMO OFDM RadCom systems	Sum-rate and energy-efficiency maximization

In other studies, optimization techniques were used to further enhance the Radcom performance. For instance, in [22], joint subcarrier and power allocation for a surveillance radar with a secondary communication function was formulated as a non-convex optimization problem which when solved provided the optimum allocations that minimize power consumption. Likewise, resource allocation in wireless-powered RadCom was optimized in [23]. A brief comparison of the aforementioned RadCom studies is presented in Table I.

Notwithstanding, most of the aforementioned studies considered joint beamforming or transmitting an integrated waveform mainly for long-range radars and communications where the round-trip time of the waves is sufficiently large to perform radar waveform transmission during downlink, and receiving the radar echos reflected from targets during uplink. Hence, a pulsed radar transmitting a high-power waveform pulse with a reasonably selected pulse-repetition time (PRT) was considered in most studies. On the other hand, in short-range radars (i.e., automotive radars), as considered in this study, the range of the radar is usually up to $R_{max} = 200$ m [26], and hence, the maximum round-trip time of the electromagnetic waves is $2R_{max}/c_0 = 1.33$ μs, where c_o denotes the speed of light. This is a very short time relative to the symbol duration of a typical OFDM system, and thus, the radar transmit and receive antennas must operate at the same time as a continuous-wave radar. Hence, in addition to interference from the communication system, this requires the self-interference between the simultaneously operating transmit and receive antennas to also be considered. In [21], we proposed a continuous-wave massive MIMO RadCom system with a novel precoder capable of interference exploitation and a waveform design that utilizes all the subcarriers for the communication and radar by transmitting an omnidirectinal OFDM waveform. Moreover, since the communication data is beamformed onto the UEs, the targets are likely to be illuminated by the radar waveform and the processing gain of the symbol-based OFDM radar is used to improve the radar detection performance. Due to the aforementioned reasons, an OFDM waveform is employed as the radar waveform, which provides high signal processing flexibility, and enables the use of the same frequency resources for sensing and communications via the proposed architecture. The proposed RadCom architecture and optimized precoders are mainly developed for future vehicular systems, where radar sensing and communications are expected to be paramount requirements, especially for autonomous driving and intelligent transportation systems.

In this study, we propose new precoder schemes that can enhance the sum-rate (SR) and energy-efficiency (EE) by optimizing the radar and communication power outputs, as well as, the beam power allocation to the UEs, without compromising the communication capacity or/and radar detection. Furthermore, we derive analytical expressions for the communication link capacity and radar SINR of our proposed RadCom architecture, [21][1], under practical network conditions where the UEs and targets may have significantly different channel gains. Moreover, we investigate the influence of other network parameters on the SR and EE of the considered RadCom system and show that the proposed schemes offer superior performance to benchmark techniques. The contributions of this study can be summarized as:

1) Proposed novel RadCom precoder schemes that maximize the communication SR and EE, while maintaining a desired radar detection performance and minimum rate per UE requirements.
2) Derived analytical expressions for the downlink communication capacity and radar SINR for our proposed RadCom, assuming randomly located UEs and targets.
3) Optimized the SR and EE of RadCom for different precoding schemes, while taking into account the communication and radar transmit powers, and number of UEs and antennas.

In the rest of this paper, Section II introduces the system model, while Section III presents the precoder and optimum radar waveform design for the RadCom system. The communication channel capacity analysis is given in Section IV. Section V presents the power consumption model, while Section VI characterizes the performance under communication interference. Section VII formulates the optimization problems to maximize SR and EE, while Section VIII presents the results and discussions. Finally, conclusions are drawn in Section IX.

Notation: Throughout the paper, the following notation is used. Bold uppercase letters (e.g. $\mathbf{H}$) indicate matrices while

[1] [21] assumed i.i.d. channel condition and UEs with the same average channel gain to simplify the analysis.

bold lowercase letters (e.g. $\mathbf{h}$) indicate vectors. Superscripts *, ^{T}, ^{H} indicate the conjugate, transpose and Hermitian transpose, respectively. Subscripts $_{com}$ and $_{rad}$ relate the corresponding parameter to communication or radar (e.g. $\mathbf{H}_{com}$ and $\mathbf{H}_{rad}$). $\mathbb{E}[.]$ and $tr[.]$ denote the expectation operator and the trace of a matrix, respectively. The absolute value, Euclidean norm and Frobenius norm operators are denoted by $|.|$, $\|.\|$ and $\|.\|_F$, respectively.

II. System Model

Fig. 1 illustrates the RadCom system under consideration, where the BS beamforms the UEs' data and omnidirectionally transmits interleaved OFDM radar waveforms via two radar transmit antennas, while the radar receive antennas receive the radar returns reflected off the targets [19]. The proposed architecture is mainly designed for the detection of near targets, and hence, includes a continuous-wave radar with simultaneously operating transmit and receive antennas. The communication antenna array beamforms data onto the UEs, while the radar antenna emits an omnidirectional OFDM radar waveform for detecting possible targets in the range, and the radar interference at the UEs is exploited. Employing separate waveforms for communications and sensing maintains communication capacity and satisfies the required radar detection performance during downlink transmission. Furthermore, all subcarriers can be used for both communications and radar sensing at the same time, and this enables highly efficient bandwidth utilization. Moreover, the interfering communication signals with the radar waveforms are substantially suppressed by symbol-based OFDM radar processing gain, and thus, the impact of the communication signals on the radar target estimation is greatly alleviated [21].

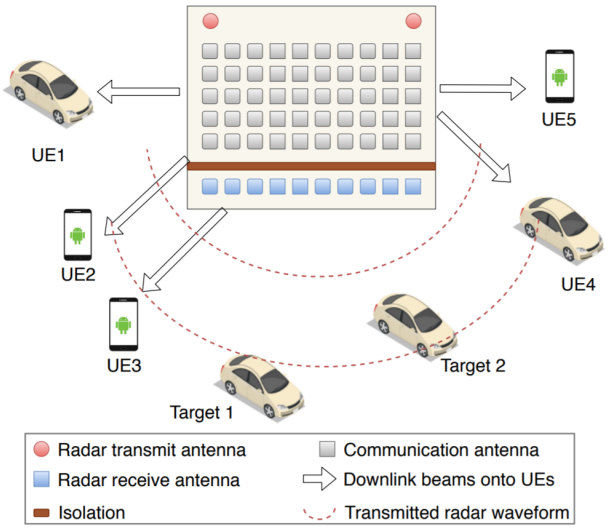

Fig. 1. A system model where the BS communicates with downlink UEs via precoding while detecting the in-range targets .

A. OFDM Radar Waveform

OFDM radars have been studied extensively recently as a promising candidate for future vehicular radars [25]. To acquire the channel state information between the radar and the targets, the OFDM waveforms emitted by the transmit antennas are compared with the waveforms reflected by the targets onto the receive antennas [18]. The transmitted radar waveform matrix, $\mathbf{S} \in \mathbb{C}^{N\times L}$, consisting of N phase-shift keying (PSK) symbols over L subcarriers is given by

$$\mathbf{S} = \begin{pmatrix} s_{1,1} & s_{1,l} & \cdots & s_{1,L} \\ s_{\mu,1} & s_{\mu,l} & \cdots & s_{\mu,L} \\ \vdots & \vdots & \ddots & \vdots \\ s_{N,1} & s_{N,l} & \cdots & s_{N,L} \end{pmatrix}, \tag{1}$$

where $s_{\mu,l}$ denotes the μth PSK symbol on the lth subcarrier.

B. Communication Channel Model

In this study, each UE is considered to be randomly located in the cell, and hence, the UEs may have different channel gains [27]. The path-loss of the kth UE is modeled as [28]

$$PL_k = 10\log_{10}\left(\frac{4\pi f_c d_0}{c_0}\right)^2 + 10\log_{10}\left(\frac{d_k}{d_0}\right)^{\varphi} + \zeta_{sh}, \tag{2}$$

where f_c, d_0, c_0 and φ denote the frequency of the carrier signal, the reference distance, the speed of light and the path-loss exponent, respectively. Moreover, d_k denotes the distance of the kth UE to the BS, (i.e. $30 \leq d_k \leq 400$ m), and ζ_{sh} denotes the log-normal shadow fading which is a zero-mean Gaussian random variable with standard deviation σ_{sh}. Based on the non-line-of-sight (NLOS) urban macrocell measurements in [28], the following parameters are used in the channel model: $f_c = 5$ GHz, $d_0 = 1$ m, $\varphi = 2.9$, $\sigma_{sh} = 5.7$ dB. On this account, the large-scale fading of the kth UE is given by $\beta_k = 10^{-PL_k/10}$. The small scale fading between the kth UE and the mth BS antenna is modeled as $f_{m,k} \sim \mathcal{CN}(0,1)$ which pertains to a Rayleigh channel model. Hence, the channel vector of the kth UE is given by $\mathbf{h}_k = \sqrt{\beta_k}\mathbf{f}_k \in \mathbb{C}^{M\times 1}$, where $\mathbf{f}_k = [f_{1,k}, \ldots f_{m,k}, \ldots, f_{M,k}]^T$. The communication channel matrix between M BS antennas and K UEs, $\mathbf{H}_{com} \in \mathbb{C}^{M\times K}$, and the radar-communication interference channel vector between the radar transmit antenna and K UEs, $\mathbf{h}_{rad} \in \mathbb{C}^{1\times K}$ are based on this model.

C. Radar Channel Model

Unlike communication channels which are generally modeled as NLOS, the channels between the radar and targets usually have strong line-of-sight (LOS) components. Moreover, radar channels are usually modeled as two-way channels, since the signals transmitted by the radar are reflected off the target, and then received by the receive antennas. Considering that U targets are present in the radar range, the channel between the radar transmit antenna, the uth target, and the qth receive antenna is modeled as [18]

$$g_{u,q} = a_{u,q} e^{-j2\pi l \Delta f \Theta_u} e^{j2\pi f_{D,u} \mu t_o}, \tag{3}$$

where $e^{-j2\pi l\Delta f\Theta_u}$ with $\Theta_u = (R_{u,tx} + R_{u,q})/c_0$ denotes the phase shift due to the total path length $(R_{u,tx} + R_{u,q})$ from the radar transmit antenna to the target, $R_{u,tx}$, and the target to the qth antenna element, $R_{u,q}$. Moreover, l and Δf denote the subcarrier index and OFDM subcarrier spacing, respectively

[18][2]. The second phase shift term given by $e^{j2\pi f_{D,u}\mu t_o}$ includes velocity information of the targets, where t_o denotes the duration of an OFDM symbol. The Doppler shift caused by the target velocity is given by $f_{D,u} = 2v_u f_c/\lambda$, where v_u denotes relative speed of the uth target, and λ denotes the wavelength of the signal. According to [29], the gain of the two-way channel between the radar transmit antenna, the uth target and the qth radar receive antenna is given by

$$a_{u,q} = \frac{\lambda\sqrt{G_{tx}G_{rx}\sigma_u}}{(4\pi)^{3/2}R_{u,tx}R_{u,q}}, \tag{4}$$

where G_{tx} and G_{rx} are the gains of the transmit and receive antennas, respectively and σ_u is the radar cross-section (RCS) of the target. Thus, the radar channel between the radar transmit antenna, targets and Q radar receive antennas is given by

$$\mathbf{g}_{rad} = \left[\sum_{u=1}^{U} g_{u,1}, \ldots, \sum_{u=1}^{U} g_{u,q}, \ldots, \sum_{u=1}^{U} g_{u,Q}\right] \in \mathbb{C}^{1\times Q}. \tag{5}$$

The communication downlink interference channel on the radar is denoted by $\mathbf{G}_{com} \in \mathbb{C}^{M\times Q}$. Each entry of the interference channel is given by $g_{m,q} = \sum_{u=1}^{U} g_{m,q,u}$, with each channel between the mth communication transmit antenna, U targets, and qth radar receive antenna calculated using (3).

D. Direct-Coupling Channel

In all continuous-wave radars, self-interference caused by direct-coupling between the antennas can be observed due to the fact that electromagnetic waves directly travel from transmit to, simultaneously operating, receive antennas. Compared to the radar and communication channels, the direct-coupling channel is modeled as slowly varying, since the locations of the antennas are fixed [30]. The direct-coupling channel vector between the single radar transmit and radar receive antennas is denoted by $\mathbf{c}_r \in \mathbb{C}^{1\times Q}$, and the direct-coupling matrix between the communication antennas and radar receive antennas is denoted by $\mathbf{C}_c \in \mathbb{C}^{M\times Q}$. Each entry of these matrices, i.e. the direct-coupling between the mth transmit and the qth receive antenna, is modeled as $c_{mq} = \Lambda_{mq}e^{(-2\pi j d_{mq}/\lambda)}$ [31], where Λ_{mq} denotes the channel gain of the direct-coupling, and d_{mq} is the distance between the mth and the qth antennas. Note that the radar receive antennas must be well-isolated from the transmit antennas to avoid saturating low-noise amplifiers connected to the receive antennas. This isolation can be achieved by a suitable antenna array design [32], where the average direct-coupling gain was measured as $\Lambda_{mq}[\text{dB}] = -70$ dB. These channel matrices can be estimated and the radar can be calibrated to cancel out the self-interference, as the transmitted signals and coupling channels are known by the BS [33]. Since communication antennas and radar transmit antennas transmit at the same time, the self-interference only affects the radar detection, and it can be removed during radar image processing [18], [21].

[2]Note that clutter is omitted in the radar model, since signal-independent clutter can be modeled as extra targets.

III. Massive MIMO OFDM RadCom Precoder

This section presents the proposed precoders and the optimum radar waveform designs.

A. Precoder Design by Exploiting Radar Interference

A single BS equipped with M antennas is assumed to communicate with K downlink UEs, while the single radar transmit antenna transmits an OFDM waveform, and the Q radar receive antennas simultaneously receive the echos reflected off U targets during the communication downlink frame[3]. The total communication and radar antenna output powers are denoted by p_{com} and p_{rad}, respectively. The transmitted symbol vector, $\mathbf{y} \in \mathbb{C}^{M\times 1}$ by M communication antennas on the lth subcarrier during one symbol duration is

$$\mathbf{y} = \sqrt{p_{com}}\alpha_{ZF}\mathbf{W}_{\text{ZF}}^{H}\mathbf{\Delta}_K\mathbf{x}, \tag{6}$$

where, a zero-forcing (ZF) precoder is employed, as given by $\mathbf{W}_{ZF}$=$\left(\mathbf{H}_{com}^{H}\mathbf{H}_{com}\right)^{-1}\mathbf{H}_{com}^{H}$, and is based on the estimated communication channel matrix. Vector $\mathbf{x} = [x_1, \ldots, x_k, \ldots, x_K]^T \in \mathbb{C}^{K\times 1}$ denotes complex quadrature amplitude modulation (QAM) symbols with average unit power, i.e. $\mathbb{E}\left[|x_k|^2\right] = 1$, which are transmitted by the BS to the K UEs. The power coefficient α_{ZF} is used to satisfy the power constraint of the precoded symbols, such that $\mathbb{E}\left[\|\mathbf{y}\|^2\right] = p_{com}$. Moreover, since the UEs are assumed to be randomly located in the network a power allocation matrix given by $\mathbf{\Delta}_K = \text{diag}\left(\sqrt{\delta_1}, \ldots, \sqrt{\delta_k}, \ldots, \sqrt{\delta_K}\right) \in \mathbb{R}^{K\times K}$ is employed in (6) to control the power beam transmitted towards each UE. This power allocation matrix must satisfy the following total power condition,

$$\sum_{k=1}^{K}\mathbb{E}\left[\left\|\mathbf{w}_k^H\right\|^2\right] = \sum_{k=1}^{K}\mathbb{E}\left[\left\|\mathbf{w}_k^H\sqrt{\delta_k}\right\|^2\right], \tag{7}$$

where $\mathbf{w}_k \in \mathbb{C}^{1\times M}$ denotes the precoder vector of the kth UE, and its average power is $\mathbb{E}\left[\|\mathbf{w}_k\|^2\right] = \frac{1}{(M-K)\beta_k}$ for the ZF precoder [34]. Thus, the following condition is obtained,

$$\sum_{k=1}^{K}\frac{1}{(M-K)\,\beta_k} = \sum_{k=1}^{K}\frac{\delta_k}{(M-K)\,\beta_k}$$
$$\sum_{k=1}^{K}\frac{1}{\beta_k} = \sum_{k=1}^{K}\frac{\delta_k}{\beta_k}. \tag{8}$$

Considering that the radar transmits an OFDM waveform with the downlink communication, the received signal vector by K UEs on the lth subcarrier under radar interference is

$$\widetilde{\mathbf{x}} = \underbrace{\mathbf{H}_{com}^{H}\mathbf{y}}_{useful\ signal} + \underbrace{\mathbf{h}_{rad}^{H}\sqrt{p_{rad}}s_{\mu,l}}_{radar\ interference} + \mathbf{n}, \tag{9}$$

where the transmitted radar symbol during this symbol duration on the lth subcarrier is denoted by $s_{\mu,l}$. Moreover, $\mathbf{n} = [n_1, \ldots, n_k, \ldots, n_K] \in \mathbb{C}^{K\times 1}$ denotes the complex Gaussian noise vector with zero mean and noise variance σ_n^2, i.e. $n_k \sim \mathcal{CN}\left(0, \sigma_n^2\right)$ at the kth UE. It can be seen in (9) that

[3]Although more radar transmit antennas may be employed, it would not change the analysis presented in this paper, as they transmit interleaved OFDM waveforms over specific subcarriers, as previously shown in [21]. Hence, only one transmit antenna is considered in the analysis for the sake of simplicity.

the radar interference at the UEs degrades the communication capacity. Therefore, the following precoder was proposed in [21] to improve the capacity of the communication system by creating constructive interference at the UEs,

$$\mathbf{y} = \sqrt{p_{com}}\widehat{\alpha}_{ZF}\mathbf{W}_{ZF}^{H}\Delta_k\mathbf{x} - \sqrt{\Psi p_{com}}\mathbf{W}_{ZF}^{H}\mathbf{h}_{rad}^{H}s_{\mu,l}, \quad (10)$$

where the first term indicates the useful communication signal and the second term indicates the signal transmitted to exploit the radar interference. Moreover, Ψ denotes the power ratio between the radar and communication output power, i.e. $p_{rad} = \Psi p_{com}$. This signal must still satisfy the output power constraint of the communication antennas, as given by

$$\mathbb{E}\left[\left\|\widehat{\alpha}_{ZF}\mathbf{W}_{ZF}^{H}\Delta_k\mathbf{x} - \sqrt{\Psi}\mathbf{W}_{ZF}^{H}\mathbf{h}_{rad}^{H}s_{\mu,l}\right\|^2\right] = 1. \quad (11)$$

Assuming that (8) is satisfied, we can exclude Δ_k from (11). In turn, $\widehat{\alpha}_{ZF}$ must be chosen as

$$\widehat{\alpha}_{ZF} = \sqrt{\frac{1 - \Psi\mathbb{E}\left[\left\|\mathbf{W}_{ZF}^{H}\mathbf{h}_{rad}^{H}\right\|^2\right]}{\mathbb{E}\left[\left\|\mathbf{W}_{ZF}\right\|_F^2\right]}}, \quad (12)$$

where $\mathbf{W}_{ZF}^{H}$ and $\mathbf{h}_{rad}^{H}$ are independent. Hence,

$$\mathbb{E}\left[\left\|\mathbf{W}_{ZF}^{H}\mathbf{h}_{rad}^{H}\right\|^2\right] \approx \mathbb{E}\left[\left\|\mathbf{W}_{ZF}^{H}\right\|_F^2\right]\mathbb{E}\left[\left\|\mathbf{h}_{rad}\right\|^2\right]\frac{1}{K}, \quad (13)$$

with $\mathbb{E}\left[\left\|\mathbf{h}_{rad}\right\|^2\right]/K$ being the average gain of the user-radar interference channels, as given by $\mathbb{E}\left[\left\|\mathbf{h}_{rad}\right\|^2\right]/K = \sum_{k=1}^{K}\frac{\beta_k}{K}$. Moreover, the Frobenius norm of ZF is calculated as

$$\mathbb{E}\left[\left\|\mathbf{W}_{ZF}^{H}\right\|_F^2\right] = \sum_{k=1}^{K}\mathbb{E}\left[\left\|\mathbf{w}_k^{H}\right\|^2\right] = \sum_{k=1}^{K}\frac{1}{(M-K)\,\beta_k}, \quad (14)$$

and therefore,

$$\Psi\mathbb{E}\left[\left\|\mathbf{W}_{ZF}^{H}\mathbf{h}_{rad}^{H}\right\|^2\right] \approx \Psi\sum_{k=1}^{K}\frac{1}{(M-K)\,\beta_k}\sum_{k=1}^{K}\frac{\beta_k}{K}. \quad (15)$$

Although each β_k can be significantly different, it can be verified that, after many network instances of randomly located UEs, this expression approximates to

$$\Psi\sum_{k=1}^{K}\frac{1}{(M-K)\,\beta_k}\sum_{k=1}^{K}\frac{\beta_k}{K} \approx \frac{\Psi K}{M-K}. \quad (16)$$

In turn, the analytical expression of $\widehat{\alpha}_{ZF}$ is given by

$$\widehat{\alpha}_{ZF} = \sqrt{(M - K - \Psi K)\left(\sum_{k=1}^{K}\frac{1}{\beta_k}\right)^{-1}}. \quad (17)$$

When $\beta_k = \beta$, $\forall k \in K$, this parameter can be simplified to

$$\widehat{\alpha}_{ZF} = \sqrt{\frac{\beta\,(M - K - \Psi K)}{K}}. \quad (18)$$

It should be noted that $\widehat{\alpha}_{ZF}$ must be greater than 0 for the communication operation, i.e. $M - K - \Psi K > 0$, and hence, the maximum radar-communication power ratio supported by the proposed scheme is given by

$$\Psi < \frac{M-K}{K}. \quad (19)$$

If the radar power is increased beyond this point, then the BS may not utilize the radar interference at the UEs.

B. Optimum Radar Waveform Design

The symbol-based radar processing scheme is employed to estimate the range and velocity of the targets, and hence, the estimation performance of the radar is independent of the transmitted symbols in the radar waveform [18], [35]. Consequently, instead of employing a random radar waveform (RRWF), an optimum radar waveform (ORWF) can be designed by minimizing the distance between the communication symbols and the radar interference received at the UEs to maximize the communication SR without affecting the radar detection. While QAM modulation is used for the communication downlink, PSK modulation is employed in the OFDM radar waveform. This is because each PSK symbol has the same amplitude, as it is necessary for radars to maintain a constant output power over all subcarriers. The optimum radar waveform can be obtained by the following optimization,

$$\underline{\mathcal{P}1:} \quad s_{\mu,l} = \underset{s_{\mu,l}}{\operatorname{argmin}} \left\|\widehat{\alpha}_{ZF}\mathbf{H}_{com}^{H}\mathbf{W}_{ZF}^{H}\Delta_k\mathbf{x} - \sqrt{\Psi}\mathbf{h}_{rad}^{H}s_{\mu,l}\right\|^2 \quad (20)$$

$$\text{s.t.} \quad \frac{\|\mathbf{S}\|_F}{NL} = 1, \quad (20b)$$

$$\left\|\widehat{\alpha}_{ZF}\mathbf{W}_{ZF}^{H}\Delta_k\mathbf{x} - \sqrt{\Psi}\mathbf{W}_{ZF}^{H}\mathbf{h}_{rad}^{H}s_{\mu,l}\right\|^2 = 1. \quad (20c)$$

It should be noted that problem $\mathcal{P}1$ can be straightforwardly solved by searching for the optimum radar symbol in the radar symbol constellation set. Also, one can verify that (20b) is inherently satisfied by transmitting a PSK-based radar waveform, with $\mathbf{S}$ being defined in (1). The optimum radar symbols will be dependent on the transmitted communication symbols and estimated channels. Hence, the transmit power constraint of the communication antennas, i.e. (20c), is satisfied by introducing a scaling factor, β_{ZF}, which is approximated by,

$$\beta_{ZF} \approx \sqrt{\mathbb{E}\left[\left\|\widehat{\alpha}_{ZF}\mathbf{W}_{ZF}^{H}\Delta_k\mathbf{x} - \sqrt{\Psi}\mathbf{W}_{ZF}^{H}\mathbf{h}_{rad}^{H}s_{\mu,l}\right\|^2\right]^{-1}}. \quad (21)$$

Selecting the optimum radar symbols reduces the power required for the radar signal cancellation, resulting in a larger part of the transmitted power by the array being allocated for the communication signal. Conseqeuntly, by inserting β_{ZF} and optimum radar symbol in (10), the transmitted signal vector with optimum radar waveform can be given by

$$\mathbf{y} = \sqrt{p_{com}}\beta_{ZF}\widehat{\alpha}_{ZF}\mathbf{W}_{ZF}^{H}\Delta_k\mathbf{x} - \mathbf{W}_{ZF}^{H}\sqrt{\Psi}\mathbf{h}_{rad}^{H}s_{\mu,l}, \quad (22)$$

where the radar waveform is optimized by (20a). Considering that the BS communicates with K UEs using the proposed precoder, and performs target detection with the optimum radar waveform target, the received signals at K UEs is given as

$$\widetilde{\mathbf{x}} = \mathbf{H}_{com}^{H}\sqrt{p_{com}}\beta_{ZF}\widehat{\alpha}_{ZF}\mathbf{W}_{ZF}^{H}\mathbf{\Delta_k}\mathbf{x} - \mathbf{H}_{com}^{H}\sqrt{\Psi p_{com}}\mathbf{W}_{ZF}^{H}\mathbf{h}_{rad}^{H}s_{\mu,l} + \mathbf{h}_{rad}^{H}\sqrt{p_{rad}}s_{\mu,l} + \mathbf{n}. \quad (23)$$

The power transmitted towards each UE can be determined by $\sqrt{\delta_k}$, and the transmitted beam vector towards the kth UE is

$$\mathbf{y}_k = \sqrt{p_{com}}\widehat{\alpha}_{ZF}\mathbf{w}_k^{H}\sqrt{\delta_k}. \quad (24)$$

$$\hat{x}_k = \sqrt{p_{com}}\left(\sqrt{\delta_k}\beta_{ZF}\widehat{\alpha}_{ZF}\mathbf{h}_{com,k}^H\mathbf{w}_k^H x_k - \sqrt{\Psi}\mathbf{h}_{com,k}^H\mathbf{w}_k^H h_{rad,k}^* s_{\mu,l}\right) + \sqrt{p_{com}}\sum_{i=1,i\neq k}^{K}\left(\sqrt{\delta_i}\beta_{ZF}\widehat{\alpha}_{ZF}\mathbf{h}_{com,k}^H\mathbf{w}_i^H x_i - \sqrt{\Psi}\mathbf{h}_{com,k}^H\mathbf{w}_i^H h_{rad,i}^* s_{\mu,l}\right) + \sqrt{p_{com}\Psi}h_{rad,k}^* s_{\mu,l} + n_k. \tag{25}$$

$$\hat{x}_k = \sqrt{p_{com}}\sqrt{\delta_k}\beta_{ZF}\widehat{\alpha}_{ZF}\mathbf{h}_{com,k}^H\mathbf{w}_k^H + \sqrt{p_{com}}\sum_{i=1,i\neq k}^{K}\mathbf{h}_{com,k}^H\mathbf{w}_i^H\left(\sqrt{\delta_i}\beta_{ZF}\widehat{\alpha}_{ZF} - \sqrt{\Psi}h_{rad,i}^*\right) + \sqrt{\Psi p_{com}}h_{rad,k}^*\left(1 - \mathbf{h}_{com,k}^H\mathbf{w}_k^H\right) + n_k. \tag{26}$$

$$SINR_k = \frac{\delta_k\beta_{ZF}^2\widehat{\alpha}_{ZF}^2\mathbb{E}\left[\left|\mathbf{h}_{com,k}^H\mathbf{w}_k^H\right|^2\right]}{\sum_{i=1,i\neq k}^{K}\mathbb{E}\left[\left|\mathbf{h}_{com,k}^H\mathbf{w}_i^H\left(\sqrt{\delta_i}\beta_{ZF}\widehat{\alpha}_{ZF} - \sqrt{\Psi}h_{rad,i}^*\right)\right|^2\right] + \Psi\mathbb{E}\left[\left|h_{rad,k}^*\right|^2\right]\mathbb{E}\left[\left|1 - \mathbf{h}_{com,k}^H\mathbf{w}_k^H\right|^2\right] + \frac{\sigma_n^2}{p_{com}}}. \tag{27}$$

Since the UEs are non-uniformly distributed in the network, the average SNR per UE is defined by $\overline{\rho} = \frac{p_{com}\overline{\beta}_k}{K\sigma_n^2}$, where $\overline{\beta}$ denotes the average channel gain of UEs, i.e. $\overline{\beta} \triangleq \sum_{k=1}^{K}\beta_k/K$. $\overline{\rho}$ is used to evaluate the capacity of the network.

IV. Derivation of the SINR Expressions

This section presents the analytical derivations used for optimizing the power allocation. It is assumed that the BS perfectly estimates the channel state information (CSI) in each coherence time by exploiting the pilot symbols transmitted by the UEs, and UE channels are uncorrelated for simplicity[4]. Accordingly, based on (23), the received signal by the kth UE is given by (25), where $\mathbf{h}_{com,k}$ denotes the channel vector of the kth UE and $h_{rad,k}$ denotes the radar interference channel with the kth UE. The first term of (25) indicates the useful signal received by the kth UE, the second term indicates the interference from the transmitted signals to the other UEs, and the third term indicates the radar interference at this UE. Moreover, the first and second terms contain the radar interference cancellation terms as subtractions. The transmitted communication symbols have unit average power, and the radar waveform symbols (i.e. PSK symbols) have unit power, such that $\mathbb{E}\left[|x_k|^2\right] = 1$, and $|s_{\mu,l}|^2 = 1$. Thus, these symbol terms are not included in the power equations. When the radar-communication output power ratio condition—in (19)—holds, (25) can be rearranged as given in (26). Based on (26), the SINR of the signal at the kth UE can be determined as given by (27).

In the case of perfect CSI and $M \gg K$, $\mathbb{E}\left[\left|\mathbf{h}_{com,k}^H\mathbf{w}_k^H\right|^2\right] = 1$ and $\mathbb{E}\left[\left|\mathbf{h}_{com,k}^H\mathbf{w}_i^H\right|^2\right] = 0$, which results in the cancellation of inter-user interference and utilization of the radar interference at the UEs [21]. By substituting $\widehat{\alpha}_{ZF}$, given by (17), into (27), the analytical approximation of the SINR at the kth UE is obtained as

$$SINR_k \approx \frac{p_{com}\delta_k\beta_{ZF}^2\left(M - K - \Psi K\right)}{\sigma_n^2}\left(\sum_{k=1}^{K}\frac{1}{\beta_k}\right)^{-1}. \tag{28}$$

If all UEs have the same large-scale fading coefficient, i.e. $\beta_k = \beta$, $\forall k \in K$, this simplifies to

$$SINR_k \approx \frac{p_{com}\delta_k\beta_{ZF}^2\beta\left(M - K - \Psi K\right)}{K\sigma_n^2}. \tag{29}$$

If RRWF is employed instead of ORWF, $SINR_k$ can then be calculated by setting $\beta_{ZF} = 1$. Employing ORWF provides higher SINR compared to the case of RRWF. This SINR gain is due to β_{ZF}^2 as illustrated in Fig. 2 with $M = 100$ BS antennas, number of UEs varies from 5 to 20, and radar-communication power ratio is in the range $0 \leq \Psi \leq 4$. With low number of UEs, i.e. $K = 5$ and a high radar power output, employing ORWF can provide nearly 50% more SINR gain to the UEs; however, having more UEs might limit this gain.

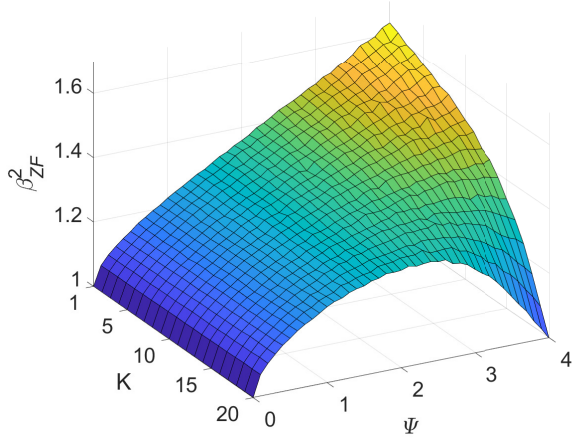

Fig. 2. ORWF SINR gain β_{ZF}^2 over RRWF versus number of UEs K, and radar-communication power ratio Ψ, for $M = 100$.

[4]The imperfect CSI case was analyzed in [21], where it was shown to degrade the communication capacity and radar detection.

V. BS Power Consumption Model

This section presents an approximate power consumption model for the radar and downlink communication of the RadCom system by taking into account the output powers of the antennas, power consumption of the radio frequency (RF) chains, amplifiers and computation units. Since it is not possible to give an exact power consumption model, we follow a similar approach to [36] to model the total consumed power. The power amplifiers (PAs) connected to the antennas are assumed to operate in the linear operation regions with a power-efficiency of $\mu_{ac} = 0.39$ for the communication PAs [36], and $\mu_{ar} = 0.3$ for the radar PA. This is because the single radar antenna is driven by a single high-power PA, while the communication antenna array elements are driven by M low-power PAs. It is well known that a high-power PA usually has lower power-efficiency than a low-power PA. Another non-negligible power loss occurs due to the impedance mismatch between the antennas and the RF chains [37]. For example, the measured total efficiency of a single antenna element—including impedance mismatch—was reported to be between $0.4-0.5$ in [37]. Accordingly, $\mu_{an} = 0.4$ is used in this study. Moreover, the RF chains include other components, such as filters, mixers, oscillators, and digital-to-analog converters (DACs), which also consume significant amounts of power. This power consumption per chain is assumed to be fixed, and denoted by p_{cr}. Hence, the total power consumed can be calculated by $(M+1)\,p_{cr}$, considering M communication antennas, and one radar transmit antenna. Moreover, the radar receiver consumes a fixed amount of power per receive antenna, denoted by p_q, which consists of the power consumed by the each receive RF chain, low-noise amplifier, and analog-to-digital converters (ADCs). In addition to the BS, the power consumed by each UE is taken into account, and is denoted by p_u per UE. Consequently, the power consumption of the system can be expressed as

$$p_{sys} = p_{base} + (M+1)\,p_{cr} + Qp_q + Kp_u + \frac{p_{com}}{\mu_{ac}\mu_{an}} + \frac{p_{rad}}{\mu_{ar}\mu_{an}}, \tag{30}$$

where p_{base} denotes the energy consumed by the CPU and the other digital hardware of the BS.

VI. OFDM Radar and Target Detection

Detection of the targets using an OFDM waveform is similar to the channel estimation widely performed in MIMO communication systems. To extract the range and velocity information of the targets, 2D Fourier transform can be applied through the frequency and time axes on the target channel information matrix, respectively [18]. The detection performance of an OFDM radar is related to the SINR of the radar signals received by the radar receive antennas, as the noise and interference in the received signals can deteriorate its detection performance. The received signal vector, $\mathbf{r}(\mu,l) = [r_1(\mu,l),\ldots,r_q(\mu,l),\ldots,r_Q(\mu,l)] \in \mathbb{C}^{Q\times 1}$, by Q radar receive antennas on the lth subcarrier with the μth transmitted symbol is given by

$$\begin{aligned}\mathbf{r}(\mu,l) = {} & p_{com}\mathbf{g}_{rad}^H \Psi s_{\mu,l} + p_{com}\mathbf{G}_{com}^H \mathbf{y} \\ & + \left(\mathbf{c}_r \Psi s_{\mu,l} + \mathbf{C}_c^H \mathbf{y}\right) + \mathbf{n}_Q,\end{aligned} \tag{31}$$

where the first term indicates the radar returns from the targets, the second term indicates the interference from the communication antennas, the third term indicates the self-interference between transmit and receive antennas, and $\mathbf{n}_Q \in \mathbb{C}^{Q\times 1}$ denotes the Gaussian noise with zero mean and variance σ_n^2 (i.e. $n_q \sim \mathcal{CN}\left(0,\sigma_n^2\right)$), since radar and UE receive chains are assumed to have the same noise variance (i.e. σ_n^2) for simplicity. It should be noted that the BS knows transmitted radar and communication symbols, and can estimate the direct-coupling matrices. Thus, the radar can be calibrated to eliminate self-interference [33], [38]. Moreover, having employed OFDM waveform, the BS can precisely estimate the self-interference in each subcarrier and cancel it out concurrently overall subcarriers. In turn, the self-interference is assumed to be canceled here for the sake of simplicity.

The radar channel between the radar transmit antenna, the target, and the qth receive antenna is estimated by element-wise division of the received signal by the transmit radar symbol, as

$$\begin{aligned}\hat{g}_{rad,q}(\mu,l) &= \frac{r_q(\mu,l)}{p_{com}\Psi s_{\mu,l}} \\ &= g_{rad,q}(\mu,l) + \frac{p_{com}\mathbf{g}_{com,q}^H \mathbf{y} + n_q}{p_{com}\Psi s_{\mu,l}}.\end{aligned} \tag{32}$$

Recall that the transmitted radar waveform matrix consists of N 16-PSK symbols over L subcarriers (i.e. $\mathbf{S} \in \mathbb{C}^{N\times L}$), and thus, a processing gain of $G_p \triangleq NL$ will be obtained after FFT/IFFT-based OFDM radar signal processing [18], [20]. Therefore, the average radar SINR per target after radar processing for the qth radar receive antenna is given by

$$\chi_{rad} = \frac{G_p p_{com}\Psi \mathbb{E}\left[\left|g_{rad,q}^* s_{\mu,l}\right|^2\right]}{U\left(p_{com}\mathbb{E}\left[\left|\mathbf{g}_{com,q}^H \mathbf{y}\right|^2\right] + \sigma_n^2\right)}, \tag{33}$$

where the power of the radar channel is calculated as

$$\mathbb{E}\left[\left|g_{rad,q}^* s_{\mu,l}\right|^2\right] = \mathbb{E}\left[\left|g_{rad,q}^*\right|^2\right], \tag{34}$$

since $\mathbb{E}\left[\left|s_{\mu,l}\right|^2\right] = 1$ for PSK symbols. The power of the communication interference on the radar return is given as

$$\begin{aligned}\mathbb{E}\left[\left|\mathbf{g}_{com,q}^H \mathbf{y}\right|^2\right] &= \mathbb{E}\left[\left|g_{com,q}^*\right|^2\right]\mathbb{E}\left[\|\mathbf{y}\|^2\right] \\ &= \sqrt{p_{com}}\,\mathbb{E}\left[\left|g_{com,q}^*\right|^2\right].\end{aligned} \tag{35}$$

Considering the radar channel model given in subsection II-C, one can show that $\mathbb{E}\left[\left|g_{rad,q}^*\right|^2\right] = \sum_{u=1}^{U} a_{u,q}^2$, and $\mathbb{E}\left[\left|g_{com,q}^*\right|^2\right] = \sum_{u=1}^{U} a_{u,q}^2$ for U targets. Hence, the analytical expression of the radar received SINR is obtained as

$$\chi_{rad} = \frac{G_p p_{com}\Psi \sum_{u=1}^{U} a_{u,q}^2}{U\left(p_{com}\sum_{u=1}^{U} a_{u,q}^2 + \sigma_n^2\right)}. \tag{36}$$

The radar returns are amplified by the radar processing gain G_p, which turns out that the communication interference is substantially suppressed by the symbol-based OFDM processing. Therefore, it is observed that the radar received SINR is mainly limited by the noise.

Fig. 3 shows the estimated velocity-distance radar images of a single target using the OFDM radar under communication

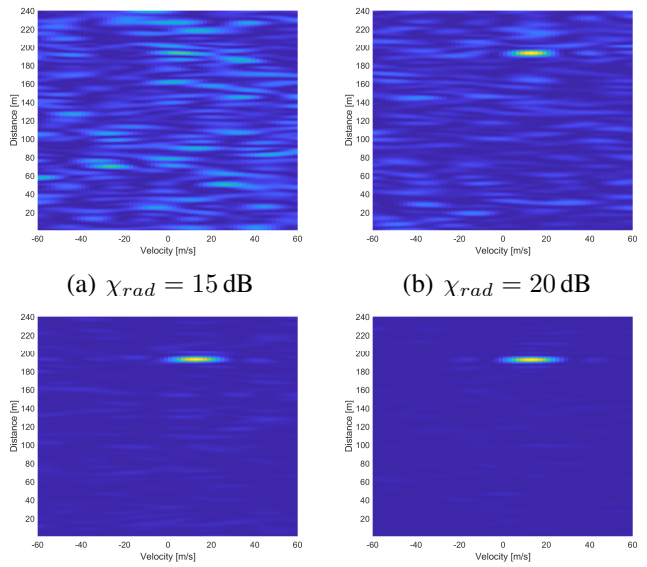

(a) $\chi_{rad} = 15$ dB (b) $\chi_{rad} = 20$ dB

(c) $\chi_{rad} = 25$ dB (d) $\chi_{rad} = 30$ dB

Fig. 3. Detection of a single target using OFDM radar with different SINRs.

interference. We consider a single target here to explicitly show how radar SINR impacts the target estimation, and this can be easily scaled to include more targets. Moreover, a multi-target scenario was considered in [21]. To obtain these radar images, 2D FFT is used as the radar processing method, as in [20]. The employed radar waveform consists of $N = 64$ 16-PSK symbols over $L = 1024$ subcarriers, and hence, the radar processing gain is $G_p = 48.2$ dB. The distance and velocity of the target are set as 200 m and 17 m/s, respectively, and the RCS of the target is $\sigma_u = 0$ dBm^2. It can be seen that the target cannot be detected easily when $\chi_{rad} < 20$ dB, and having higher SINR provides better detection performance by decreasing the shadow targets caused by the interference and noise. Thus, the radar image SINR should be greater than 20 dB for a reasonable target detection performance. Accordingly, the minimum radar image SINR constraint is set as $\chi_{rad} \geq 25$ dB, while optimizing the precoder to satisfy target detection requirements. To obtain 25 dB radar image gain, the SINR of the received radar signals must be at least $\chi_{rad} - G_p = -23.2$ dB with this specific radar waveform. The RCS of vehicles typically vary between 0 dBm^2 and 25 dBm^2, depending on the size, shape and materials used on the surface of the vehicle [39]. To increase the sensitivity of the radar, we consider that the radar must be able to detect the objects with 0 dBm^2 RCS within the detection range. Hence, $\sigma_u = 0$ dBm^2 is accepted in the analysis and simulations. Taking into account this minimum radar image SINR requirement, the power of the communication beams and total power output of the RadCom BS is optimized in the next sections to improve the spectral and energy efficiencies of the RadCom system. Signal parameter estima- tion for passive bistatic radar with waveform correlation exploitation

VII. Optimum Beam Power Allocation

This section presents the optimization of the communication and radar output powers, and the power beamed at the UEs to maximize SR and EE of the RadCom system. The ZF precoder utilizes the pseudoinverse of the channel matrix for beamforming, and thus it tends to equalize the received powers at the UEs. However, this may limit the spectral and energy efficiencies of the system, as more power would be allocated to the beams towards the UEs with the worst channel conditions. Moreover, the radar antenna output power must be carefully chosen to ensure that the targets can be detected without affecting the downlink communication. The analytical expressions derived in the previous sections will be used here to simplify the optimum power allocation problems. Note that radar waveform design and beam power optimization, which require only estimated CSI, are performed at the BS during CSI estimation stage and before downlink in each TDD frame.

A. Sum-Rate Maximization

Maximizing SR must be done in conjunction with satisfying the minimum required SINR for radar detection, minimum rate per UE, and the transmit power constraint of the communication and radar antennas. Assuming p_{com} is fixed, the maximum SR can be achieved by solving problem $\mathcal{P}2$ formulated as

$$\underline{\mathcal{P}2:} \tag{37}$$

$$\max_{\Delta_K, \Psi} \; C_{sum}\left(\Delta_K, \Psi\right) = \sum_{k=1}^{K} C_k\left(\delta_k, \Psi\right) \tag{37a}$$

$$\text{s.t.} \quad p_{rad} = \Psi p_{com}, \tag{37b}$$

$$\chi_{rad}\left(\Psi\right) \geq \chi_{min}, \tag{37c}$$

$$C_k\left(\delta_k, \Psi\right) \geq C_{min}, \quad \forall k = 1, \ldots, K, \tag{37d}$$

$$\sum_{k=1}^{K} \frac{1}{\beta_k} \geq \sum_{k=1}^{K} \frac{\delta_k}{\beta_k}, \tag{37e}$$

$$\delta_k \geq 0, \quad \forall k = 1, \ldots, K, \tag{37f}$$

$$\Psi \geq 0, \tag{37g}$$

where C_k is the achievable rate of the kth UE, expressed as

$$C_k\left(\delta_k, \Psi\right) = B \log_2\left(1 + SINR_k\left(\delta_k, \Psi\right)\right), \tag{38}$$

with $SINR_k$ being defined in (28) for the case of randomly located UEs, and (29) for the case of equal UEs channel gains. Moreover, C_{min} is the minimum rate requirement per UE.

In $\mathcal{P}2$, constraint (37b) determines the radar power output, while (37c) ensures that the minimum radar SINR is satisfied to detect the targets with the minimum target radar cross-section σ_{min} within the radar range R_{max}. Constraint (37d) ensures that each UE satisfies C_{min}, while (37f) ensures that the optimum power allocation does not change the total transmit power of the BS antennas. The last two constraints define the range of values the decision variables can take.

It can be easily verified that the rate function of each UE is non-convex in (δ_k, Ψ), which can be verified from the SINR expression of each UE and the fact that Ψ affects the calculation of $\widehat{\alpha}_{ZF}$ and β_{ZF}. This implies that problem $\mathcal{P}2$ is non-convex, and hence, is computationally-intensive. To

$$\mathrm{EE}\left(\Delta_K,\Psi\right)=\frac{C_{sum}\left(\Delta_K,\Psi\right)}{p_{sys}\left(\Psi\right)}=\frac{B\sum_{k=1}^{K}\log_2\left(1+SINR_k\right)}{p_{base}+\left(M+1\right)p_{cr}+Qp_q+Kp_u+\dfrac{p_{com}}{\mu_{ac}\mu_{an}}+\dfrac{\Psi p_{com}}{\mu_{ar}\mu_{an}}}. \tag{41}$$

alleviate the complexity of problem $\mathcal{P}2$, χ_{rad} in (36) can be used to determine the minimum value of Ψ, as

$$\Psi_{min}=10^{\chi_{min}/10}\left(\frac{U\left(p_{com}\sum_{u=1}^{U}a_{u,q}^2+\sigma_n^2\right)}{p_{com}G_p\sum_{u=1}^{U}a_{u,q}^2}\right), \tag{39}$$

where $a_{u,q}$ is given by (4), which includes the target range R_u and radar cross-section σ_u. By setting $R_u=R_{max}$ and $\sigma_u=\sigma_{min}$, the minimum radar-communication power ratio, Ψ_{min}, can be computed, and thus, $\Psi\geq\Psi_{min}$. This ensures that the radar power output is sufficient to provide the desired radar image SINR, while keeping it as low as possible to avoid higher radar interference at the UEs, and reduce the power consumption.

In turn, constraint (37c) becomes redundant, and hence can be eliminated from problem $\mathcal{P}2$. In practical systems, the ratio of the radar output power to the communication output (i.e. $p_{rad}=\Psi p_{com}$) can be fixed, while ensuring that $\Psi\geq\Psi_{min}$, which implies that constraint (37b) can also be eliminated from problem $\mathcal{P}2$. Thus, problem $\mathcal{P}2$ can be simplified, and reformulated as

$$\underline{\mathcal{P}3:} \tag{40}$$

$$\max_{\Delta_K}\ C_{sum}\left(\Delta_K\right)=\sum_{k=1}^{K}C_k\left(\delta_k\right) \tag{40a}$$

$$\text{s.t.}\quad C_k\left(\delta_k\right)\geq C_{min},\quad \forall k=1,\ldots,K, \tag{40b}$$

$$\sum_{k=1}^{K}\frac{1}{\beta_k}\geq\sum_{k=1}^{K}\frac{\delta_k}{\beta_k}, \tag{40c}$$

$$\delta_k\geq 0,\quad \forall k=1,\ldots,K. \tag{40d}$$

For fixed Ψ (hence $p_{rad}=\Psi p_{com}$), it can be easily verified that the rate function of each UE is concave in δ_k, which implies that constraint (40b) is concave, and the objective function $C_{sum}\left(\Delta_K\right)$ is also concave in Δ_K, since it is a linear sum of concave functions. Also, (40c) is linear in Δ_K, since it is a linear sum of δ_k. Consequently, problem $\mathcal{P}3$ is a concave maximization problem, and hence can be solved efficiently and globally optimally within polynomial-time complexity of $\mathcal{O}\left(K^2\right)$ via any standard optimization package [40].

In summary, to solve problem $\mathcal{P}2$, the minimum value of Ψ (i.e. Ψ_{min}) must first be determined. Then, the system designer can select an appropriate value of $\Psi\geq\Psi_{min}$, which is followed by the solution of problem $\mathcal{P}3$, which in turn maximizes SR for the selected value of Ψ. Alternatively, to find the optimal solution (Δ_k,Ψ), the system designer can increase the value of Ψ in small increments, starting from Ψ_{min}, and then solve problem $\mathcal{P}3$ to obtain Δ_K for each value of Ψ. After that the optimal combination of (Δ_k,Ψ) that yields the maximum SR value can be determined, as will be demonstrated in Section VIII.

B. Energy-Efficiency Maximization

The system's EE is defined as the ratio of the SR to the total power consumption, given by (41), where p_{sys} is as given in (30). Various parameters, such as output power of antennas, power consumption of the BS internal circuitry, number of UEs, can affect EE. Moreover, maximizing SR does not necessarily maximize EE, as power consumption of the system will also increase with the increase in SR. In turn, the system's EE can be maximized by solving problem $\mathcal{P}4$, which is formulated as

$$\underline{\mathcal{P}4:} \tag{42}$$

$$\max_{\Delta_K,\Psi}\ \mathrm{EE}\left(\Delta_K,\Psi\right) \tag{42a}$$

$$\text{s.t.}\quad \text{Constraints } (37b)-(37g). \tag{42b}$$

As before, it can be straightforwardly shown that $\mathcal{P}4$ is non-convex, and hence is computationally-intensive. To simplify problem $\mathcal{P}4$, it can be verified that the increase in Ψ decreases EE. Specifically, there are two main reasons for this decrease in EE, which are the low-efficiency power amplifier connected the radar transmit antenna, and omnidirectinal transmission of the radar waveform. For this reason, the minimum value of Ψ (i.e. Ψ_{min}) that satisfies the desired radar detection performance should be chosen by setting $\Psi=\Psi_{min}$, where Ψ_{min} is given by (39). Consequently, when p_{com} is fixed, $p_{rad}=\Psi_{min}p_{com}$. In turn, the total power consumption can be expressed as

$$\begin{aligned}\overline{p}_{sys}&\triangleq p_{sys}\left(\Psi_{min}\right)\\&=p_{base}+\left(M+1\right)p_{cr}+Qp_q+Kp_u\\&\quad+\frac{p_{com}}{\mu_{ac}\mu_{an}}+\frac{\Psi_{min}p_{com}}{\mu_{ar}\mu_{an}},\end{aligned} \tag{43}$$

while the SR function can be defined as

$$\overline{C}_{sum}\left(\Delta_K\right)\triangleq C_{sum}\left(\Delta_K,\Psi_{min}\right). \tag{44}$$

In turn, the EE function in (41) can be re-expressed as

$$\overline{\mathrm{EE}}\left(\Delta_K\right)=\frac{\overline{C}_{sum}\left(\Delta_K\right)}{\overline{p}_{sys}}. \tag{45}$$

Therefore, problem $\mathcal{P}4$ can be reformulated as

$$\underline{\mathcal{P}5:} \tag{46}$$

$$\max_{\Delta_K,\Psi}\ \overline{\mathrm{EE}}\left(\Delta_K\right) \tag{46a}$$

$$\text{s.t.}\quad \text{Constraints } (40b)-(40d). \tag{46b}$$

$\mathcal{P}5$ is an equivalent transformation of $\mathcal{P}4$, since every increase in Ψ beyond Ψ_{min} can be verified to decrease the EE. Similar to problem $\mathcal{P}3$, it can be easily verified that problem $\mathcal{P}5$ is a concave maximization problem, which can be solved globally optimally within polynomial-time complexity of $\mathcal{O}\left(K^2\right)$ [40].

C. Complexity Analysis

The computational complexity of the proposed schemes is presented in terms of floating-point operations (FLOPs). While each operation for real numbers requires 1 FLOP, each

complex operation (e.g. complex multiplication, summation, square-root) requires 2 FLOPs. The computation of the ZF precoder (i.e. computing $\mathbf{W}_{ZF}$) requires pseudoinversing the complex channel matrix, and two complex matrix-matrix multiplications, which can be completed in approximately $\mathcal{O}(6MK^2)$ [41] [42]. ZFR-RRWF requires the calculation of (10), which includes the ZF precoder and (17). The calculation of (17) requires only $(2K+6)$ FLOPs, as it includes only scalar values. Consequently, the complexity of ZFR-RRWF is calculated as $(6MK^2+2K+6)$. ZFR-ORWF requires the computation of $\mathcal{P}1$ and (21), in addition ZFR-RRWF. The computation of $\mathcal{P}1$ requires $(8ZK+Z)$ FLOPs, where Z denotes the constellation size of the PSK modulation (e.g., $Z=16$ for 16-PSK) employed in the radar waveform. Moreover, the computation of (21) requires only $(2K+2)$ FLOPs, since most values used in this equation were already calculated in the previous equations. Therefore, the computation of the ZFR-ORWF scheme requires $(6MK^2+8ZK+4K+Z+8)$ FLOPs. Since the analytical expressions simplified the power allocation problems, $\mathcal{P}3$ and $\mathcal{P}5$ turned out to be concave, thus can be solved with polynomial-time complexity of $\mathcal{O}(K^2)$ [40], which is the extra complexity required for computing ZFR-RRWF-OP and ZFR-ORWF-OP, in addition to the complexity of the ZFR-RRWF or ZFR-ORWF schemes. The complexity of the proposed schemes is summarized in Table II, while omitting the constant parts of the complexity expressions. It can be seen that the complexity is dominated by the computation of ZF ($\mathbf{W}_{ZF}$), which suggests that the proposed RadCom precoders do not entail excessive computational burden, hence can be implemented in real-time applications.

Table II
COMPUTATIONAL COMPLEXITIES

Scheme	Complexity [FLOPs]
ZF	$6MK^2$
ZFR-RRWF	$6MK^2+2K$
ZFR-ORWF	$6MK^2+8ZK+4K+Z$
ZFR-RRWF-OP	$6MK^2+K^2+2K$
ZFR-ORWF-OP	$6MK^2+8ZK+K^2+4K+Z$

VIII. NUMERICAL RESULTS

This section presents the optimized SR and EE performance of the proposed RadCom precoders for different parameters[5].

A. Simulation Parameters

The simulation parameters are given in Table III, where the subcarrier spacing is selected at least 10 times higher than the maximum Doppler shift to alleviate the mutual interference between adjacent subcarriers [18], [19]. It is assumed that the desired maximum detectable target range is $R_{max}=200$ m for a target with RCS $\sigma_u=0$ dBm^2, as in vehicular radars [26]. While the radar range is 200 m, the range of the communication cell radius is set as 400 m, since the BS may need to provide service to the UEs in a larger area. Note that the noise variance in dBm is calculated as $\sigma_n^2[\text{dBm}]=N_0+NF+10\log_{10}B$, where $NF=7$ dB denotes the noise figure of the receivers. Hence, the noise variance in Watts is given by $\sigma_n^2=10^{\left(\sigma_n^2[\text{dBm}]-30\right)/10}$. The numerical results are averaged over 1000 random network instances.

[5]As $\mathcal{P}3$ and $\mathcal{P}5$ happen to be nonlinear concave maximization optimization problems, they are solved via CVX [43].

Table III
PARAMETERS OF THE RADCOM SYSTEM

Parameter	Value	Description
p_{base}	21 W	BS base power consumption
p_{cr}	0.5 W	Power of each RF chain
p_u	1 W	Power of each UE during downlink
p_q	1 W	Power cons. per radar receive antenna
μ_{an}	0.4	Total antenna efficiency
μ_{ac}	0.39	Communication PA efficiency
μ_{ar}	0.3	Radar PA efficiency
B	100 MHz	Bandwidth
L	1024	Number of subcarriers
N	64	Number of symbols per radar waveform
T_{sym}	10.2 μs	Elementary symbol duration
T_{cp}	1.33 μs	Cyclic-prefix duration
T_O	11.53 μs	OFDM symbol duration
N_0	-174 dBm/Hz	Noise spectral density
σ_u	0 dBm^2	Target radar cross-section

In the numerical results, the following schemes are defined based on the proposed precoder, optimum radar waveform design and beam power allocation. Particularly, ZFR-ORWF and ZFR-RRWF indicate the proposed ZF-based radar interference utilization precoder (ZFR) with the optimum radar waveform (ORWF), and random radar waveform (RRWF), respectively. Moreover, ZFR-ORWF-OP and ZFR-RRWF-OP refer to the aforementioned schemes but with the optimum power (OP) allocation without a minimum rate constraint per UE. Note that aggressively striving to reach the maximum SR or EE might force the BS not to beamform any data onto the UEs with the worst channel conditions. To avoid this, we defined a minimum rate constraint C_{min} for each UE, as per problems $\mathcal{P}3$ and $\mathcal{P}5$. Consequently, ZFR-ORWF-OP $(C_k \geq C_{min})$ and ZFR-RRWF-OP $(C_k \geq C_{min})$ indicate the minimum rate constraint is enforced per UE in the ZFR-ORWF-OP and ZFR-RRWF-OP schemes, respectively. Finally, ZF-WRI indicates the ZF precoder with radar interference, while ZF-WORI indicates the ZF precoder without considering the radar interference.

B. Comparative Results

The accuracy of the analytical SR and radar SINR expressions derived in Sections IV and VI are examined in Fig. 4, which shows a good agreement between the analytical and simulations results for all values of Ψ with all schemes. It can also be seen that increasing the radar-communication ratio Ψ with the assistance of the radar processing gain G_p rapidly improves the radar SINR χ_{rad}, since the transmitted radar power also increases (i.e. $p_{rad}=\Psi p_{com}$). On the other hand, a

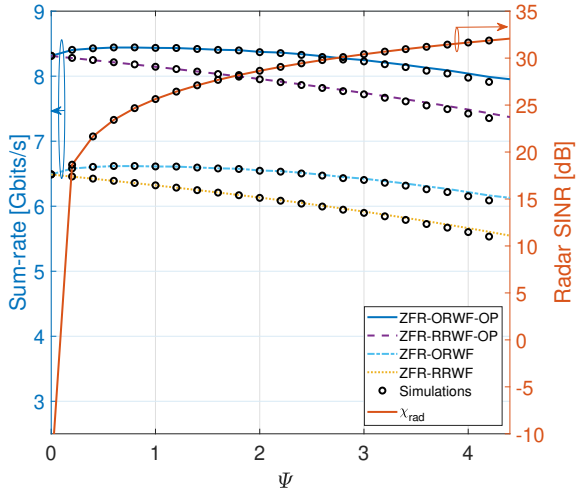

Fig. 4. Analytical and simulation results of SR w.r.t. radar-communication power ratio. $M = 100$, $K = 10$, $P_{com} = 10$ W.

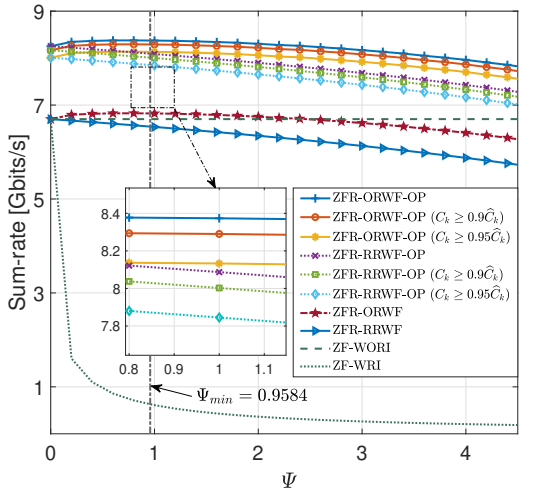

(a) $K = 10$ UEs

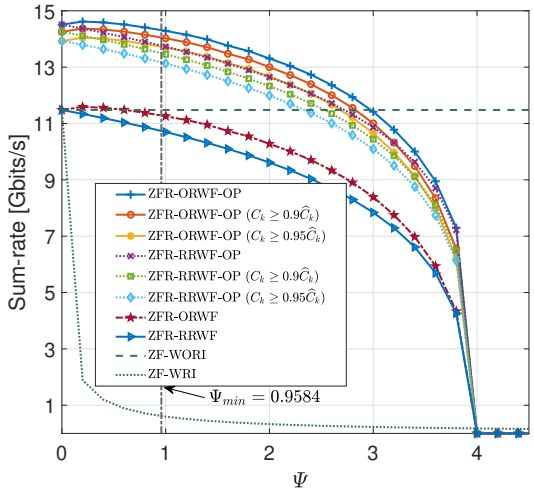

(b) $K = 20$ UEs

Fig. 5. SR of RadCom w.r.t increasing radar-communication power ratio. $M = 100$, $p_{com} = 10$ W.

substantial SR gain is obtained when the optimum beam power allocation is employed, as seen in the comparison between ZFR-ORWF and ZFR-ORWF-OP, and also between ZFR-RRWF and ZFR-RRWF-OP. It is also observed that increasing the radar-communication power ratio Ψ to a certain value ($\Psi < 1$) improves the SR when ZFR-ORWF and ZFR-ORWF-OP are employed, as they can utilize the radar interference. On the other hand, excessively increasing Ψ degrades SR due to the subsequent increase in radar interference, which may not be utilized entirely due to the limited power output of the communication antennas[6].

In Fig. 5, maximizing the SR is investigated under minimum rate constraints per UE. Two minimum rate constraints are examined, i.e., $C_{min} = 0.9\widehat{C}_k$ and $C_{min} = 0.95\widehat{C}_k$, where $\widehat{C}_k$ denotes the rate of the UEs that can be achieved without beam power allocation (i.e. via the ZFR-ORWF or ZFR-RRWF schemes). The ZFR-ORWF-OP scheme outperforms all the other schemes, however, it does not guarantee that each UE can achieve the minimum rate requirement. Enforcing a minimum rate constraint slightly decreases the optimized SR, as seen in the comparison between ZFR-ORWF-OP and ZFR-ORWF-OP ($C_k \geq C_{min}$) and between ZFR-RRWF-OP and ZFR-RRWF-OP ($C_k \geq C_{min}$) in Figs. 5a and 5b. Hence enforcing this constraint reduces the feasible region of $\mathcal{P}3$, which in turn marginally decreases SR. Moreover, increasing the radar output power (via $p_{rad} = \Psi p_{com}$) up to a certain value improves SR with the ZFR-ORWF, ZFR-ORWF-OP and ZFR-ORWF-OP ($C_k \geq C_{min}$) schemes, depending on the number of UEs. For instance, for $K = 10$ UEs, the maximum SR is achieved at $\Psi = 0.8$, while for $K = 20$ UEs, the maximum SR value is achieved at $\Psi = 0.2$ as seen in Figs. 5a and b. However, further increase in Ψ causes excessive radar interference that may not be constructively utilized, and thus degrades the SR. Notably, the minimum radar-communication power ratio Ψ_{min} is found as $\Psi_{min} = 0.9584$ when $p_{com} = 10$ W, which is required to achieve the minimum radar SINR to reliably detect the target, as per Constraint (37c), i.e., $\Psi \geq \Psi_{min}$. The ZF-WORI is substantially outperformed by other schemes in terms of SR, since the ZF-WORI does not perform optimum power allocation over the beams, nor consider the radar interference. Additionally, communicating with $K = 10$ UEs allows the BS to emit higher radar power output and utilize it as useful energy source while having $K = 20$ UEs restricts the maximum emitted radar power as seen in the comparison between Figs. 5a and 5b, which is also in agreement with the maximum utilizable radar power output limit given by (19). Particularly, for $K = 10$ UEs, $\Psi < 9$, while for $K = 20$ UE, $\Psi < 4$. This explains why SR, with all schemes (other than ZF-WRI), goes to zero when $\Psi = 4$ in Fig. 5b. Lastly, utilizing the ORWF provides a significant capacity gain over RRWF. For instance, a significant SR gain of about 1.5 Gbits/s with $K = 10$, and 3 Gbits/s with $K = 20$ are observed between ZFR-ORWF-OP

[6]In [21], we compared the proposed ZFR-ORWF and ZFR-RRWF precoders with the separated and shared antenna deployments presented in [16], and showed that the proposed precoders outperform them in terms of communication capacity.

and ZFR-ORWF, and between the ZFR-RRWF-OP and ZFR-RRWF schemes. This signifies the importance of the optimal radar waveform design for the proposed precoder along with optimum downlink beam power allocation for maximizing SR in massive MIMO RadCom systems.

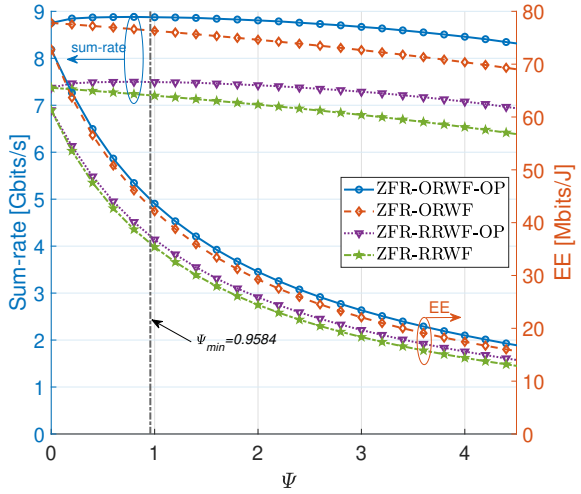

Fig. 6. SR and EE w.r.t. Ψ. $M = 100$, $K = 10$, $p_{com} = 10$ W.

After evaluating SR, the optimum EE of the RadCom system is investigated. The SR and EE of the system as a function of Ψ are illustrated in Fig. 6, where -OP signifies the optimum beam power allocation for maximizing EE. It is evident that every increase in Ψ decreases EE, which proves that selecting the minimum possible value of Ψ enhances EE, while providing reliable target detection. Moreover, one can see that the ORWF improves EE in comparison to the RRWF scheme, and further improvement can be achieved via the optimum beam power allocation. The minimum required Ψ is $\Psi_{min} = 0.9584$ for this specific network setup, where the RadCom system still closely achieves the maximum SR; however, EE significantly drops since the power transmitted by the radar antennas is included in the consumed power by the BS when calculating EE, as given in (41).

The EE of the system as a function of the communication power output under the aforementioned minimum rate constraints is examined in Fig. 7. Specifically, maximum EE is achieved when $p_{com} = 6$ W. While ZFR-ORWF-OP achieves the maximum EE, as would be expected, ZFR-ORWF-OP with $(C_k \geq 0.9\widehat{C}_k)$ and $(C_k \geq 0.95\widehat{C}_k)$ provide slightly lower EEs. This is because the aforementioned two schemes strive to satisfy the minimum rate for all UEs. Moreover, the EE of ZF-WRI is substantially degraded by the radar interference, while the ZFR-ORWF scheme provides similar EE to ZF-WORI which is a radar interference-free system. This figure proves that jointly optimizing the radar waveform and beam powers substantially enhances the EE of RadCom systems.

Fig. 8 presents EE for various numbers of UEs, using ZFR-ORWF-OP $(C_k \geq 0.9\widehat{C}_k)$ and ZFR-RRWF-OP $(C_k \geq 0.9\widehat{C}_k)$. It also illustrates the minimum required radar-communication power ratio Ψ_{min} as a function of p_{com} to satisfy the minimum radar performance. For example, while $\Psi_{min} = 0.9584$ when

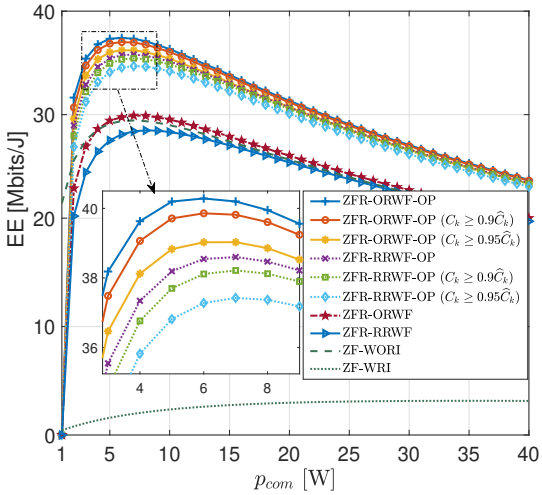

Fig. 7. EE of RadCom with different precoding schemes. $M = 100$, $K = 10$.

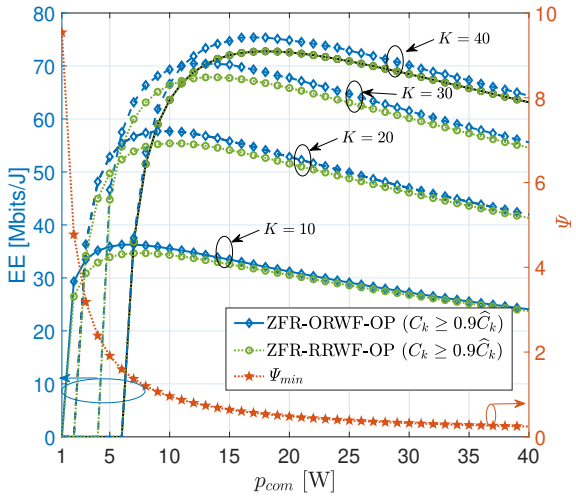

Fig. 8. Optimum EE of RadCom with different number of UEs. $M = 100$.

$p_{com} = 10$ W, only $\Psi_{min} = 0.4816$ is required to satisfy the radar performance when $p_{com} = 20$ W. On the other hand, it can be seen that having more UEs enhances EE, but requires more transmit power p_{com} to achieve the maximum EE. For instance, $p_{com} = 17$ W is required for $K = 40$ UEs, while $p_{com} = 9$ W is sufficient for $K = 20$ UEs to achieve the maximum EE.

Fig. 9a and 9b respectively show SR and EE when varying the numbers of BS antennas and UEs when ZFR-ORWF-OP $C_k \geq 0.9\widehat{C}_k$ is employed. It is worth noting that the $M > K$ condition must be satisfied for communicating with the UEs, as the ZF is employed; otherwise, the sum-rate is nulled, as shown in Fig. 9. The SR improves with the increase in the number of antennas M when the number of UEs K is fixed due to the increasing massive MIMO gain. While SR and EE improve as the numbers of BS antennas and UEs increase, keeping the number of UEs fixed while significantly increasing the number of antennas lowers EE. This is because each antenna needs a separate RF chain, which would increase the power consumed by the BS. In turn, the increase in the

power consumption outweighs the increase in the sum-rate, and hence a degradation in the EE is observed. As a result, to maintain the maximum EE, some antennas may be turned off when the number of UEs is small. This is independent of the precoder design, since the optimum RadCom precoders (ZFR-ORWF-OP and ZFR-RRWF-OP) always provide higher SR or EE with any number of antennas compared to standard precoders (ZFR-ORWF and ZFR-RRWF).

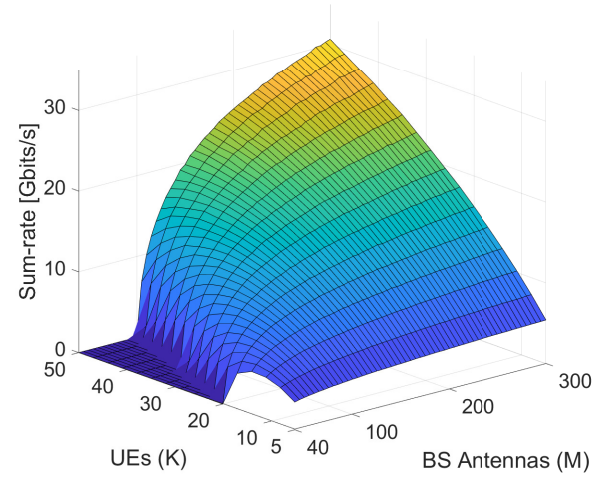

(a) SR

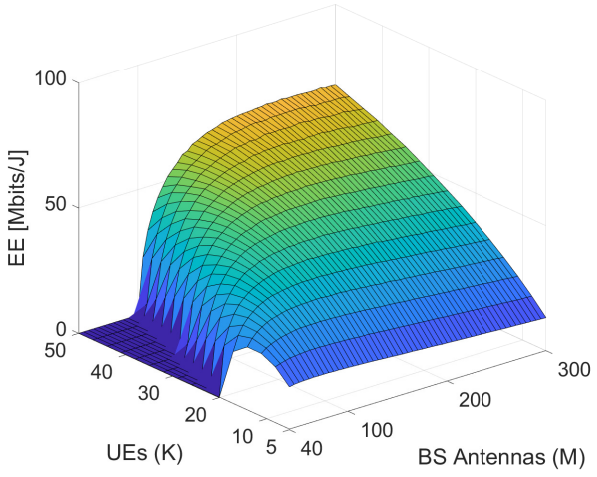

(b) EE

Fig. 9. Optimized SR and EE of RadCom with various number of BS and antennas and UEs. $\Psi = 1$ and $\overline{\rho} = 15$ dB.

IX. Conclusion

This study has presented optimized massive MIMO OFDM RadCom precoders for practical network scenarios where the UEs and targets are randomly located in the network and have random channel gains. Firstly, analytical expressions for the communication capacity and radar SINR have been derived. Using these expressions, the beam power allocation, radar-communication power ratio, and communication power output have been optimized to maximize the network SR and EE, while guaranteeing a desired radar target detection SINR and UEs' minimum rate requirements. The validity of the analytical results and proposed schemes have been validated via extensive numerical simulations. It was shown that the proposed precoders substantially benefit from the optimum radar waveform design and optimum beam power allocation, in addition to exploiting the radar interference to enhance SR and EE. Lastly, the presented complexity analysis of the proposed schemes have demonstrated that the computational requirement is modest, making them viable options for real-time RadCom systems. Future extension of this work will consider multi-cell RadCom networks, including cell-free MIMO with inter-cell interference management and sharing of sensing information between the UEs.

Acknowledgement

This work was partially supported by the Ministry of National Education of Turkey and the Kuwait Foundation for the Advancement of Sciences (KFAS) under project code PN17-15EE-02.

References

[1] B. Paul, A. R. Chiriyath, and D. W. Bliss, "Survey of RF communications and sensing convergence research," *IEEE Access*, vol. 5, pp. 252–270, 2017.

[2] A. R. Chiriyath, B. Paul, and D. W. Bliss, "Radar-communications convergence: Coexistence, cooperation, and co-design," *IEEE Trans. on Cogn. Commun. Netw.*, vol. 3, no. 1, pp. 1–12, Mar. 2017.

[3] R. Saruthirathanaworakun, J. M. Peha, and L. M. Correia, "Opportunistic sharing between rotating radar and cellular," *IEEE J. Sel. Areas Commun.*, vol. 30, no. 10, pp. 1900–1910, Nov. 2012.

[4] S. Sodagari, A. Khawar, T. C. Clancy, and R. McGwier, "A projection based approach for radar and telecommunication systems coexistence," in *Proc. IEEE Global Communications Conference (GLOBECOM)*, Dec. 2012, pp. 5010–5014.

[5] J. A. Mahal, A. Khawar, A. Abdelhadi, and T. C. Clancy, "Spectral coexistence of MIMO radar and MIMO cellular system," *IEEE Trans. Aerosp. Electron. Syst.*, vol. 53, no. 2, pp. 655–668, Apr. 2017.

[6] B. Li, A. P. Petropulu, and W. Trappe, "Optimum co-design for spectrum sharing between matrix completion based MIMO radars and a MIMO communication system," *IEEE Trans. Signal Process.*, vol. 64, no. 17, pp. 4562–4575, Sep. 2016.

[7] F. Liu, C. Masouros, A. Li, T. Ratnarajah, and J. Zhou, "MIMO radar and cellular coexistence: A power-efficient approach enabled by interference exploitation," *IEEE Trans. Signal Process.*, vol. 66, no. 14, pp. 3681–3695, July 2018.

[8] J. Qian, Z. He, N. Huang, and B. Li, "Transmit designs for spectral coexistence of MIMO radar and MIMO communication systems," *IEEE Trans. Circuits Syst. II Express Briefs*, vol. 65, no. 12, pp. 2072–2076, Dec 2018.

[9] F. Wang, H. Li, and M. A. Govoni, "Power allocation and co-design of multicarrier communication and radar systems for spectral coexistence," *IEEE Trans. Signal Process.*, vol. 67, no. 14, pp. 3818–3831, July 2019.

[10] Q. Li, K. Dai, Y. Zhang, and H. Zhang, "Integrated waveform for a joint radar-communication system with high-speed transmission," *IEEE Wireless Commun. Lett.*, vol. 8, no. 4, pp. 1208–1211, Aug. 2019.

[11] Z. Geng, R. Xu, H. Deng, and B. Himed, "Fusion of radar sensing and wireless communications by embedding communication signals into the radar transmit waveform," *IET Radar, Sonar Nav.*, vol. 12, no. 6, pp. 632–640, 2018.

[12] Y. Liu, G. Liao, J. Xu, Z. Yang, and Y. Zhang, "Adaptive OFDM integrated radar and communications waveform design based on information theory," *IEEE Commun. Lett.*, vol. 21, no. 10, pp. 2174–2177, Oct. 2017.

[13] Q. Zhang, Y. Zhou, L. Zhang, Y. Gu, and J. Zhang, "Waveform design for a dual-function radar-communication system based on CE-OFDM-PM signal," *IET Radar, Sonar Nav.*, vol. 13, no. 4, pp. 566–572, Apr. 2019.

[14] S. D. Blunt, P. Yatham, and J. Stiles, "Intrapulse radar-embedded communications," *IEEE Trans. Aerosp. Electron. Syst.*, vol. 46, no. 3, pp. 1185–1200, July 2010.

[15] D. Ciuonzo, A. De Maio, G. Foglia, and M. Piezzo, "Intrapulse radar-embedded communications via multiobjective optimization," *IEEE Trans. Aerosp. Electron. Syst.*, vol. 51, no. 4, pp. 2960–2974, Oct 2015.

[16] F. Liu, C. Masouros, A. Li, H. Sun, and L. Hanzo, "MU-MIMO communications with MIMO radar: From co-existence to joint transmission," *IEEE Trans. Wireless Commun.*, vol. 17, no. 4, pp. 2755–2770, Apr. 2018.

[17] F. Liu, L. Zhou, C. Masouros, A. Li, W. Luo, and A. Petropulu, "Toward dual-functional radar-communication systems: Optimal waveform design," *IEEE Trans. Signal Process.*, vol. 66, no. 16, pp. 4264–4279, Aug. 2018.

[18] C. Sturm and W. Wiesbeck, "Waveform design and signal processing aspects for fusion of wireless communications and radar sensing," *Proc. IEEE*, vol. 99, no. 7, pp. 1236–1259, July 2011.

[19] C. Sturm, Y. L. Sit, M. Braun, and T. Zwick, "Spectrally interleaved multi-carrier signals for radar network applications and multi-input multi-output radar," *IET Radar, Sonar Nav.*, vol. 7, no. 3, pp. 261–269, Mar. 2013.

[20] Y. L. Sit, B. Nuss, and T. Zwick, "On mutual interference cancellation in a MIMO OFDM multiuser radar-communication network," *IEEE Trans. Veh. Technol.*, vol. 67, no. 4, pp. 3339–3348, Apr. 2018.

[21] M. Temiz, E. Alsusa, and M. W. Baidas, "A dual-functional massive MIMO OFDM communication and radar transmitter architecture," *IEEE Trans. Veh. Technol.*, vol. 69, no. 12, pp. 14 974–14 988, Dec. 2020.

[22] C. Shi, Y. Wang, F. Wang, S. Salous, and J. Zhou, "Joint optimization scheme for subcarrier selection and power allocation in multicarrier dual-function radar-communication system," *IEEE Syst. J.*, pp. 1–12, 2020.

[23] Y. Zhou, H. Zhou, F. Zhou, Y. Wu, and V. C. M. Leung, "Resource allocation for a wireless powered integrated radar and communication system," *IEEE Wireless Commun. Lett.*, vol. 8, no. 1, pp. 253–256, June 2019.

[24] M. Temiz, E. Alsusa, and L. Danoon, "Impact of imperfect channel estimation and antenna correlation on quantised massive multiple-input multiple-output systems," *IET Commun.*, vol. 13, no. 9, pp. 1262–1270, June 2019.

[25] G. Hakobyan and B. Yang, "High-performance automotive radar: A review of signal processing algorithms and modulation schemes," *IEEE Signal Process. Mag.*, vol. 36, no. 5, pp. 32–44, Sep. 2019.

[26] P. Kumari, J. Choi, N. Gonzalez-Prelcic, and R. W. Heath, "IEEE 802.11ad-based radar: An approach to joint vehicular communication-radar system," *IEEE Trans. Veh. Technol.*, vol. 67, no. 4, pp. 3012–3027, Apr. 2018.

[27] M. Temiz, E. Alsusa, L. Danoon, and Y. Zhang, "On the impact of antenna array geometry on indoor wideband massive MIMO networks," *IEEE Trans. Antennas Propag.*, vol. 69, no. 1, pp. 406–416, Jan. 2021.

[28] S. Sun and et al., "Investigation of prediction accuracy, sensitivity, and parameter stability of large-scale propagation path loss models for 5G wireless communications," *IEEE Trans. Veh. Technol.*, vol. 65, no. 5, pp. 2843–2860, May. 2016.

[29] M. A. Richards, J. A. Scheer, and W. A. Holm, Eds., *Principles of Modern Radar: Basic principles*. Institution of Engineering and Technology, 2010.

[30] T. Snow, C. Fulton, and W. J. Chappell, "Transmit-receive duplexing using digital beamforming system to cancel self-interference," *IEEE Trans. Microw. Theory Techn.*, vol. 59, no. 12, pp. 3494–3503, Dec. 2011.

[31] X. Chen, S. Zhang, and Q. Li, "A review of mutual coupling in MIMO systems," *IEEE Access*, vol. 6, pp. 24 706–24 719, 2018.

[32] B. Nuss, L. Sit, M. Fennel, J. Mayer, T. Mahler, and T. Zwick, "MIMO OFDM radar system for drone detection," in *Proc. 18th International Radar Symposium (IRS)*, 2017, pp. 1–9.

[33] E. Ahmed and A. M. Eltawil, "All-digital self-interference cancellation technique for full-duplex systems," *IEEE Trans. Wireless Commun.*, vol. 14, no. 7, pp. 3519–3532, July 2015.

[34] H. Q. Ngo, E. G. Larsson, and T. L. Marzetta, "Energy and spectral efficiency of very large multiuser MIMO systems," *IEEE Trans. Commun.*, vol. 61, no. 4, pp. 1436–1449, Apr. 2013.

[35] C. Sturm, T. Zwick, W. Wiesbeck, and M. Braun, "Performance verification of symbol-based OFDM radar processing," in *IEEE Radar Conference*, 2010, pp. 60–63.

[36] E. Bjornson, L. Sanguinetti, J. Hoydis, and M. Debbah, "Optimal design of energy-efficient multi-user MIMO systems: Is massive MIMO the answer?" *IEEE Trans. Wireless Commun.*, vol. 14, no. 6, pp. 3059–3075, June 2015.

[37] G. J. Hayes, J. So, A. Qusba, M. D. Dickey, and G. Lazzi, "Flexible liquid metal alloy (EGaIn) microstrip patch antenna," *IEEE Trans. Antennas Propag.*, vol. 60, no. 5, pp. 2151–2156, May. 2012.

[38] A. Masmoudi and T. Le-Ngoc, "Channel estimation and self-interference cancelation in full-duplex communication systems," *IEEE Trans. Veh. Commun.*, vol. 66, no. 1, pp. 321–334, Jan. 2017.

[39] T. Schipper, J. Fortuny-Guasch, D. Tarchi, L. Reichardt, and T. Zwick, "RCS measurement results for automotive related objects at 23-27 GHz," in *Proc. 5th European Conference on Antennas and Propagation (EUCAP)*, Apr. 2011, pp. 683–686.

[40] S. Boyd and L. Vandenberghe, *Convex Optimization*. Cambridge University Press, 2003.

[41] S. Huang, H. Yin, H. Li, and V. C. M. Leung, "Decremental user selection for large-scale multi-user MIMO downlink with zero-forcing beamforming," *IEEE Wireless Commun. Lett.*, vol. 1, no. 5, pp. 480–483, Oct. 2012.

[42] R. Hunger, "Floating point operations in matrix-vector calculus," Institute for Signal Processing, The Technical University of Munich, Tech. Rep. v1.3, September 2007. [Online]. Available: https://mediatum.ub.tum.de/doc/625604/625604

[43] M. Grant and S. Boyd, "CVX: Matlab software for disciplined convex programming, version 2.1," http://cvxr.com/cvx, Mar. 2014.

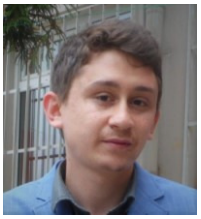

Murat Temiz (S'19-M'20) received B.S. degree in Electronics and Computer Science with Education from Gazi University and M.S. degree in Electrical and Electronics Engineering from TOBB University of Economics and Technology, respectively, both in Ankara, Turkey. He has completed his Ph.D. in Electrical and Electronic Engineering at the University of Manchester, UK. His current research interests are massive MIMO systems, antenna and antenna array design, channel measurements, optimization, dual-functional MIMO OFDM radar-communication systems and machine learning applications.

Emad Alsusa (M'06-SM'07) completed a PhD in Telecommunications from the University of Bath in the United Kingdom in 2000 and in the same year he was appointed to work on developing high data rates systems as part of an industrial project based at Edinburgh University. He joined Manchester University (then UMIST) in September 2003 as a faculty member where his current rank is a Reader in the Communication Engineering Group. His research interests lie in the area of Communication Systems with a focus on Physical, MAC and Network Layers including developing techniques and algorithms for array signal detection, channel estimation and equalization, adaptive signal precoding, interference avoidance through novel radio resource management techniques, cognitive radio and energy and spectrum optimization techniques.

Mohammed W. Baidas (M'05-SM'17) received the B.Eng. (Hons.) degree in communication systems engineering from the University of Manchester, Manchester, U.K., in 2005, the M.Sc. degree (with distinction) in wireless communications engineering from the University of Leeds, Leeds, U.K., in 2006, the M.S. degree in electrical engineering from the University of Maryland, College Park, MD, USA, in 2009, and the Ph.D. degree in electrical engineering from Virginia Tech, Blacksburg, VA, USA, in 2012. He is currently an Associate Professor with the Department of Electrical Engineering, Kuwait University, Kuwait. His research interests include resource allocation and management in cognitive radio systems, game theory, cooperative communications and networking, and green and energy-harvesting networks.